Available online at www.sciencedirect.com
ScienceDirect
Journal of Catalysis 248 (2007) 89–100
JOURNAL OF CATALYSIS
www.elsevier.com/locate/jcat

Fischer–Tropsch synthesis over γ-alumina-supported cobalt catalysts: Effect of support variables

Øyvind Borg [a], Sigrid Eri [b], Edd A. Blekkan [a], Sølvi Storsæter [a,b], Hanne Wigum [b], Erling Rytter [a,b], Anders Holmen [a,*]

[a] *Department of Chemical Engineering, Norwegian University of Science and Technology (NTNU), NO-7491 Trondheim, Norway*
[b] *Statoil R&D, Research Centre, Postuttak, NO-7005 Trondheim, Norway*

Received 4 August 2006; revised 19 February 2007; accepted 8 March 2007

Abstract

A systematic study of the effect of γ-Al_2O_3 support variables on Fischer–Tropsch synthesis activity and selectivity was carried out at industrially relevant conditions ($T = 483$ K, $P = 20$ bar, $H_2/CO = 2.1$). A total of 13 catalysts were prepared by incipient wetness impregnation of γ-Al_2O_3 supports of varying pore characteristics and chemical purities with aqueous solutions containing the required amounts of cobalt and rhenium precursor to give nominal loadings of 20 and 0.5 wt%, respectively. The catalysts were analysed for cobalt, rhenium, nitrogen, and sodium and characterised by nitrogen adsorption/desorption, mercury intrusion, X-ray diffraction, hydrogen chemisorption, temperature-programmed reduction, and oxygen titration. The size of the Co_3O_4 cobalt particles was controlled by the support pore size, with small particles formed in narrow pores and large particles formed in wide pores. The degree of reduction increased with increasing catalyst pore size and Co_3O_4 particle size. The catalysts contained different amounts of sodium (20–113 ppm) and the site-time yield decreased with increasing sodium content. Positive correlations were found between cobalt particle size and C_{5+} selectivity and between catalyst pore size and C_{5+} selectivity. The results indicate that the C_{5+} selectivity is controlled by the size and appearance of cobalt particles.

Keywords: Fischer–Tropsch synthesis; Cobalt; Rhenium; Alumina; Particle size; Pore size; C_{5+} selectivity

1. Introduction

Cobalt is considered the most favourable metal for the synthesis of long-chain hydrocarbons from natural gas-based synthesis gas because of its high activity, high selectivity to linear paraffins, high resistance toward deactivation, and low water–gas shift activity. To maximise the exposure of cobalt to gaseous reactants, the metal is normally dispersed on a high surface area support. The choice of support is important for the final Fischer–Tropsch synthesis catalyst. In particular, the pore characteristics of the support have a significant effect on the Co_3O_4 crystallite size measured after impregnation and calcination. For instance, according to Xiong et al. [1], large γ-Al_2O_3 pore sizes enhance the formation of large Co_3O_4 crystallites. Similar findings have been reported for silica-supported cobalt [2–8].

In some cases, the support interacts strongly with the active phase. Metal–support interactions may leave a fraction of the cobalt chemically inactive after reduction. Khodakov et al. [4–6] and Saib et al. [3] reported higher reducibility for wide-pore silica-supported catalysts than for cobalt deposited on narrow-pore supports. This is not surprising, because larger particles (in wide pores) are expected to behave more like bulk Co_3O_4 with respect to their reducibility than smaller particles. Khodakov et al. [9] found the ease of reduction to decrease from larger (20–70 nm) to smaller (6 nm) silica-supported Co_3O_4 particles. In contrast, Xiong et al. [1] reported a negative correlation between the Co_3O_4 particle size (and pore size) and the degree of reduction for γ-Al_2O_3-supported cobalt catalysts. The metal–support interactions can to some extent be controlled by modification of the support [10]. However, all

* Corresponding author. Fax: +47 73 59 50 47.
E-mail address: anders.holmen@chemeng.ntnu.no (A. Holmen).

0021-9517/$ – see front matter
doi:10.1016/j.jcat.2007.03.008

of the cobalt precursor is usually not transformed into metallic cobalt during reduction. To reduce the amount of nonreduced, inactive cobalt, a small amount of a second metal, such as rhenium, can be introduced into the catalyst system [11]. The general consensus is that rhenium catalyses the reduction of cobalt species interacting with the support. Hilmen et al. [12] concluded that rhenium promotes reduction by hydrogen spillover, and that no direct contact between cobalt and rhenium is needed to obtain the promoting effect. Also note that the presence of rhenium has been shown to increase the selectivity to long-chain hydrocarbons during Fischer–Tropsch synthesis [13,14].

Because the support is very important for the properties of the final Fischer–Tropsch catalyst, the activity is indirectly affected by the support nature. However, at conditions favouring chain-growth, site-time yields on supported cobalt catalysts are traditionally considered independent of cobalt dispersion and of support identity [14–20]. Thus, the catalyst productivity can be directly predicted from the number of cobalt atoms exposed on the surface. Iglesia et al. [15–17] found constant site-time yield for the cobalt particle size range 10–210 nm, which includes most of the typical low-dispersion cobalt Fischer–Tropsch catalysts. Storsæter et al. [14] also found constant site-time yield for cobalt deposited on different metal oxides (γ-Al_2O_3, SiO_2, TiO_2). However, for cobalt supported on carbon nanofibers, it has recently been shown that the site-time yield is lower for particles smaller than 8 nm [21].

The effect of the support material on the product selectivity is not well established. Iglesia et al. [15,22,23] proposed that the differences in selectivity observed for cobalt on different supports are due to variations in the extent of α-olefin readsorption. Dispersion, support, and bimetallic effects are not considered to influence the probability of intrinsic chain growth on cobalt surfaces [15,22,23]. Shi and Davis [24], on the other hand, reported that diffusion limitations for the α-olefin products and their subsequent reincorporation as chain initiators do not have major impacts on the product distribution. Bezemer et al. [21] recently reported a strong influence of the cobalt particle size on the performance in Fischer–Tropsch synthesis. The cobalt particles were deposited on inert carbon nanofiber support materials. At industrially relevant Fischer–Tropsch synthesis conditions, the C_{5+} selectivity decreased from 85 to 51% when the cobalt particle size was reduced from 16 to 3 nm.

To summarise, although the catalytic performance of cobalt supported on a large number of supports has been thoroughly investigated, the effect of support material on methane and C_{5+} selectivity remains controversial. In our opinion, some of the variations reported in the literature may be due to different conditions during catalyst preparation, reduction, and Fischer–Tropsch synthesis. Consequently, the purpose of the present study is to investigate the role of support in a highly systematic way. Furthermore, to acquire a powerful and reliable data material, a large number of catalysts (13) were prepared on supports of the same chemical identity using exactly the same preparation method and amount of active components. This allowed a systematic study of the impact of the support variables (e.g., physical parameters and chemical purity) on activity and selectivity. Moreover, product selectivity of all catalysts was compared at the same CO conversion level.

2. Experimental

2.1. Catalyst preparation

A series of 13 supported catalysts (C-1 to C-13) containing 20 wt% cobalt and 0.5 wt% rhenium were prepared by one-step incipient wetness co-impregnation of different γ-Al_2O_3 supports (S-1 to S-13) with aqueous solutions of cobalt nitrate hexahydrate, $Co(NO_3)_2{\cdot}6H_2O$, and perrhenic acid, $HReO_4$. The supports (53–90 μm) were precalcined in flowing air at 773 K for 10 h before impregnation. The samples were heated from ambient temperature to 773 K at a rate of 1 K/min.

All catalysts were dried at 393 K for 3 h after impregnation. Calcination at 573 K for 16 h in flowing air completed the preparation process. The temperature was increased from ambient temperature to 573 K at a rate of 2 K/min. Finally, the samples were sieved, and the 53–90 μm fraction was collected. Further pretreatment was done in situ.

Three other catalysts were prepared using exactly the same procedure as for S/C-1 to S/C-13 except omitting the support calcination step. In these cases, the Al_2O_3 phase of the supports (and catalysts) was different. One support was boehmite (Vista), and the other two supports were mixtures of γ, θ, and δ-Al_2O_3 (Sasol).

2.2. Support and catalyst characterisation

2.2.1. Inductively coupled plasma atomic/optical emission spectroscopy

The calcined samples (0.2 g, 53–90 μm) were analysed for sodium, cobalt, and rhenium content. The amount of metal was measured with an IRIS advantage duo inductively coupled plasma atomic/optical emission spectrometer (Thermo-Jarrel Ash). The samples were dissolved in a nitric acid solution before analysis.

2.2.2. Nitrogen adsorption/desorption

Nitrogen adsorption/desorption isotherms were measured on a Micromeritics TriStar 3000 instrument, and the data were collected at liquid nitrogen temperature (77 K). The samples (0.3 g, 53–90 μm) were outgassed at 573 K overnight before measurement.

The surface area was calculated from the Brunauer–Emmett–Teller (BET) equation [25], and the total pore volume and pore size distribution were found by applying the Barrett–Joyner–Halenda (BJH) method [26]. The nitrogen desorption branch was chosen for pore size analysis [27].

2.2.3. Mercury intrusion

Pore size measurements were performed by mercury intrusion using a Carlo Erba Porosimeter 2000. The samples (1 g, 53–90 μm) were evacuated and dried at 423 K before analysis. A cylindrical pore model was assumed.

2.2.4. X-ray diffraction

X-ray diffraction patterns were recorded for all the supports and catalysts at ambient temperature on a Siemens D5005 X-ray diffractometer using Cu$K\alpha$ radiation ($\lambda = 1.54 \times 10^{-10}$ m). The samples were crushed before measurement. The scans were recorded in the 2θ range between 10° and 90° using a step size of 0.04° and a step time of 15 s. Peaks were identified by comparison with standards in a database [28].

The average cobalt oxide crystallite thickness was calculated from Scherrer's equation [29] using the (311) Co_3O_4 peak located at $2\theta = 36.9°$. A K factor of 0.89 was used in Scherrer's formula [29,30]. To obtain a high signal-to-noise ratio and, consequently, minimise the experimental error, new scans were recorded only in the 2θ range between 32° and 43°. The step size was still 0.04°, but the step time was increased to 150 s. Lanthanum hexaboride was used as reference material to determine the instrumental line broadening. The average spherical Co_3O_4 particle size was calculated multiplying the crystallite thickness by a factor of 4/3 [31].

The Co_3O_4 particle size was converted to the corresponding cobalt metal particle size according to the relative molar volumes of metallic cobalt and Co_3O_4. The resulting conversion factor for the diameter $d(Co_3O_4)$ of a given Co_3O_4 particle being reduced to metallic cobalt is [32],

$$d(Co^0) = 0.75 \times d(Co_3O_4). \quad (1)$$

It is known, however, that cobalt oxide particles may crack during reduction in H_2 [33,34], and in such a case relation (1) is not valid.

2.2.5. Hydrogen chemisorption

Hydrogen adsorption isotherms were recorded on a Micromeritics ASAP 2010 unit at 312 K. The samples (0.5 g, 53–90 μm) were evacuated at 312 K for 1 h, and then reduced in situ in flowing hydrogen at 623 K for 16 h. The temperature was increased by 1 K/min from 312 to 623 K. After reduction, the samples were evacuated for 1 h at 603 K and for 30 min at 373 K before cooling to 312 K. The adsorption isotherm was recorded in the pressure interval ranging from 20 to 510 mm Hg. The amount of chemisorbed hydrogen was determined by intrapolating the straight-line portion of the isotherm to zero pressure. Furthermore, to calculate the dispersion, it was assumed that two cobalt surface atoms are covered by one hydrogen molecule [35], and that rhenium does not contribute to the amount of hydrogen adsorbed.

The cobalt metal particle size was calculated from the cobalt metal dispersion by assuming spherical, uniform cobalt metal particles with site density of 14.6 at/nm^2 [36]. These assumptions give the following formula:

$$d(Co^0)\ (\text{nm}) = \frac{96}{D(\%)}. \quad (2)$$

2.2.6. Temperature-programmed reduction

Temperature-programmed reduction (TPR) experiments were performed in a U-shaped tubular quartz reactor heated by an electric furnace [37]. The calcined samples (0.2 g, 53–90 μm) were exposed to a reducing gas mixture consisting of 7% H_2 in argon while the temperature was increased at 10 K/min from ambient to 1203 K.

TPR profiles were also recorded after in situ reduction of the catalysts. In this case, the calcined samples (0.2 g, 53–90 μm) were reduced in a flow of pure hydrogen at 623 K. A ramp rate of 1 K/min was used to increase the temperature from ambient to 623 K. The temperature was held at 623 K for 16 h before subsequently cooling to 298 K. The catalysts were flushed with He for 1 h, and finally heated at a rate of 10 K/min to 1203 K in 7% H_2 in Ar.

A cold trap containing a mixture of 2-propanol and dry ice was used to eliminate water and other condensable products from the product gas mixtures. The consumption of hydrogen was measured by comparing the thermal conductivity of the reference and product gas. Calibration was done by reduction of Ag_2O powder.

TPR was also used to estimate the degree of reduction. For the calcined catalysts, some of the cobalt remained as cobalt nitrate after calcination, and this was taken into account in the calculations. The hydrogen consumption of the reduced samples was also considered when the degree of reduction was calculated.

For one catalyst (C-11), TPR was performed on a Micromeritics AutoChem II instrument connected to a Pfeiffer Vacuum ThermoStar mass spectrometer. The sample was subjected to 10% H_2 in Ar while the temperature was increased from 300 to 1353 K at 10 K/min. To remove water, the reduction products were passed through a cold trap consisting of 2-propanol and liquid nitrogen. The dry reduction mixture was subsequently analysed for the common fragment ions of NO and NO_2. The hydrogen consumption was measured by comparison of the thermal conductivity of the reference and product gas.

2.2.7. Nitrogen content

A total of four calcined catalysts and one uncalcined catalyst (0.1 g, 53–90 μm) were analysed for nitrogen content. The samples were placed in a tin capsule and combusted in a high-temperature resistance furnace by raising the temperature from 1073 to 3023 K at a rate of 11 K/min. Formation of gaseous nitrogen was detected by a thermal conductivity detector in a LECO TC-436 DR unit.

2.2.8. Oxygen titration

Oxygen titration was performed using the equipment described in Section 2.2.6. The catalyst samples (0.1 g, 53–90 μm) were reduced in situ under flowing hydrogen for 16 h at 623 K. The temperature was linearly ramped from ambient temperature to 623 K at a rate of 1 K/min. The samples were flushed in flowing He at 623 K for 1 h and subsequently heated to 673 K at 5 K/min, keeping the same gaseous atmosphere. A series of pulses of oxygen were passed through the catalyst bed at 673 K [38]. The amount of oxygen consumed by the samples was calculated from the known pulse volume and the number of pulses reacting with the sample. The degree of reduction was calculated assuming that all cobalt in metallic form was

oxidised to Co_3O_4. Any oxidation of Re to Re_2O_7 was not considered in the calculations.

2.3. Activity and selectivity measurements

Fischer–Tropsch synthesis was performed in a fixed-bed reactor (stainless steel, 10 mm i.d.). The apparatus has been described in detail elsewhere [39]. The samples (1.0 g, 53–90 μm) were diluted with inert silicon carbide particles (4.0 g, 75–150 μm) to improve the temperature distribution along the catalytic zone.

The samples were reduced in situ in hydrogen at 1 bar while the temperature was increased by 1 K/min to 623 K. After 16 h of reduction, the catalysts were cooled to 443 K. The system was then pressurised to 20 bar, and synthesis gas of molar ratio $H_2/CO = 2.1$ (and 3% N_2 as internal standard) was introduced into the reactor. To avoid runaway and catalyst deactivation at startup, the temperature was increased slowly to the reaction temperature of 483 K.

Each experiment was divided into two periods, of 26 and 104 h. The following conditions were used:

Period 1: Synthesis gas at a flow rate of 250 N mL/min,
Period 2: Synthesis gas at an adjusted flow rate to give a target CO conversion of 50%.

Heavy hydrocarbons were collected in a heated trap (363 K), and liquid products were removed in a cold trap (298 K). The effluent gaseous product was analysed for hydrogen, nitrogen, carbon monoxide, carbon dioxide, water, and C_1–C_9 hydrocarbons using an HP5890 gas chromatograph equipped with a thermal conductivity detector and a flame ionisation detector.

Activity is reported as cobalt-time yield (mol CO/(mol Co × s)). C_{5+} selectivity was calculated by subtracting the amount of C_1–C_4 hydrocarbons and CO_2 in the product gas mixture from the total mass balance.

3. Results and discussion

3.1. Support and catalyst characterisation

3.1.1. Chemical catalyst composition

All of the catalysts contained a nominal amount of 20 wt% cobalt and 0.5 wt% rhenium, calculated assuming reduced catalysts with complete reduction of cobalt and rhenium. The actual metal loading was determined by ICP-AES. The results are summarised in Table 1. Analysis of the calcined catalysts gave Co and Re amounts of 16.3–18.9 wt% and 0.36–0.42 wt%, respectively. The nominal loadings were calculated assuming completely reduced catalysts, whereas ICP-AES samples were obtained from calcined catalysts containing Co_3O_4. It can be shown that 20 wt% Co on a reduced catalyst corresponds to 18.7 wt% on a completely oxidised sample. A similar rationale can be given for Re. However, most of the metal loadings were slightly lower than the recalculated nominal loadings.

As shown in Table 1, the 13 alumina supports came from different suppliers (Süd-Chemie, Alcoa, Sasol, Akzo, Harshaw) and contained different amounts of trace elements (e.g., Na, Ti, and Si). These elements were naturally also present in the impregnated samples. With respect to Fischer–Tropsch synthesis performance, the most important trace element is sodium [40]. The amount of sodium found in the calcined catalysts as determined by ICP-OES ranged from 20 to 113 ppm (Table 1). It should also be mentioned that the cobalt and rhenium precursor contained negligible amounts of sodium.

Table 1
Cobalt, rhenium, and sodium amounts. ICP-A/OES was done on the calcined samples

Sample	Support supplier	Metal content		
		Co (wt%)	Re (wt%)	Na (ppm)
C-1	Süd-Chemie	16.6	0.37	27
C-2	Alcoa	16.8	0.38	70
C-3	Sasol	16.3	0.40	26
C-4	Akzo	18.3	0.40	50
C-5	Alcoa	N.A.	N.A.	113
C-6	Alcoa	17.1	0.40	35
C-7	Sasol	17.6	0.36	26
C-8	Akzo	17.2	0.37	53
C-9	Harshaw	18.9	0.41	55
C-10	Sasol	16.8	0.40	20
S-11	Sasol	N.A.	N.A.	22
C-11	Sasol	17.7	0.42	26
C-12	Sasol	16.3	0.36	N.A.
C-13	Sasol	N.A.	N.A.	N.A.

The experimental error ($\pm 2\sigma$) for the measurements is approximately ±5% of the absolute values. S-2, S-5, S6: Alcoa HiQ series. S-4: Puralox SCCa-40/195. S-7: Pural series. S-10, S-11: Puralox SCCa series. S-12, S-13: Puralox TH high pore volume series.

3.1.2. Nitrogen adsorption/desorption

The BJH model [26] was chosen for calculation of pore sizes. Fig. 1 gives the pore size distributions of the Al_2O_3 supports and the corresponding impregnated samples. Most of the samples had a narrow Gaussian-like unimodal pore size distribution. However, some samples showed a broad (S/C-4, S/C-5, S/C-7) or bimodal (S/C-9, S/C-10, S/C-11) distribution. Table 2 shows that the surface areas were 114–262 m^2/g, the average pore diameters were 5.9–26.7 nm, and the pore volumes were 0.31–0.98 cm^3/g. Introduction of cobalt precursor significantly decreased all of the physical quantities, as shown in Table 2. The loss in initial surface area and pore volume on impregnation and calcination averaged 19 and 35%, respectively. Deposition of cobalt on the supports did not influence the shape of the pore size distribution, but merely reduced the nitrogen uptake, as shown in Fig. 1.

3.1.3. Mercury intrusion

To detect large pores (macropores) that cannot be studied by nitrogen sorption, mercury intrusion was performed for a selection of supports and catalysts. The results are presented in Table 2. In most cases, the mercury intrusion cumulative pore volumes were similar to or lower than the volumes calculated from nitrogen sorption data, essentially proving that all of the pores were detected in the latter technique. Thus, no macrop-

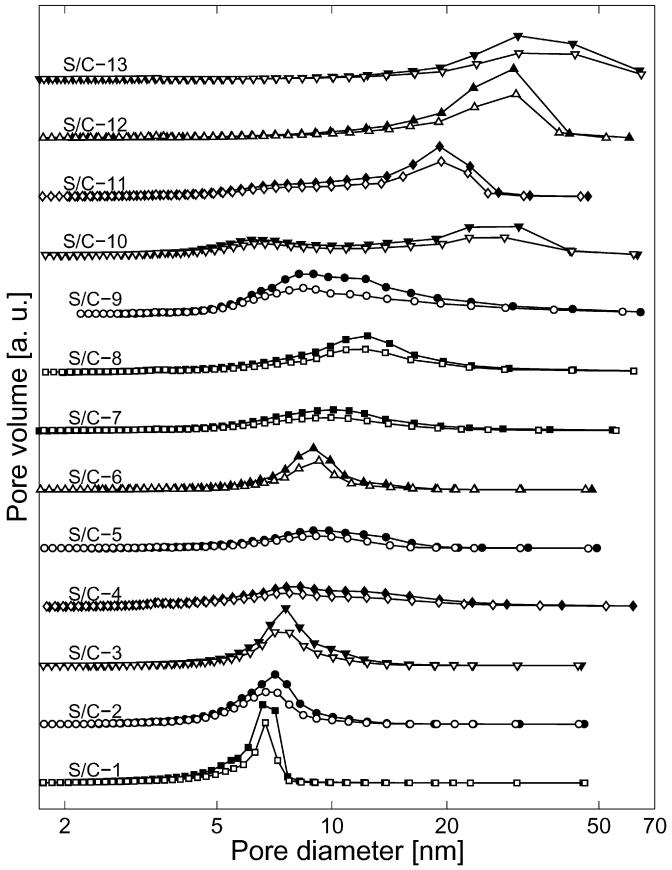

Fig. 1. Support and catalyst pore size distributions calculated from the nitrogen desorption branches using the Barrett–Joyner–Halenda method (filled symbol = support, open symbol = catalyst).

Table 2
Nitrogen sorption and mercury intrusion data for the γ-Al_2O_3 supports (S) and the impregnated samples (C)

Sample	N_2 sorption			Hg intrusion
	BET surface area (m^2/g)	Average pore diameter (nm)	Pore volume (cm^3/g)	Pore volume (cm^3/g)
S-1	232	5.9	0.46	
C-1	168	5.7	0.28	
S-2	204	6.5	0.46	
C-2	175	6.1	0.31	
S-3	184	7.4	0.48	
C-3	143	7.1	0.30	
S-4	190	8.6	0.51	
C-4	165	7.9	0.34	
S-5	103	9.0	0.31	
C-5	86	7.9	0.19	
S-6	129	8.4	0.37	
C-6	112	8.1	0.24	
S-7	161	9.0	0.44	
C-7	136	8.2	0.30	
S-8	205	10.5	0.67	
C-8	169	10.2	0.47	
S-9	262	10.6	0.93	
C-9	193	10.4	0.61	
S-10	191	11.6	0.78	0.76
C-10	149	11.6	0.51	0.51
S-11	186	12.3	0.73	
C-11	148	11.6	0.50	0.45
S-12	155	20.8	0.98	
C-12	123	18.3	0.62	0.65
S-13	114	26.7	0.86	
C-13	92	23.7	0.57	0.76

For the nitrogen sorption data, the experimental error ($\pm 2\sigma$) is ± 5 m^2/g for the surface areas, ± 0.2 nm for the average pore diameters, and ± 0.02 cm^3/g for the pore volumes. The uncertainty is based on three independent runs of all the samples.

ores ($d_p \geqslant 50$ nm) were observed for these samples. The only exception was catalyst C-13.

3.1.4. X-ray diffraction

X-ray diffraction patterns of all supports confirmed the presence of only γ-Al_2O_3 [28]. One example (S-11) is presented in Fig. 2a. This diffractogram is representative of all of the supports. The pattern of the corresponding impregnated sample (C-11) is shown in Fig. 2b. Besides the γ-Al_2O_3 peaks, the catalyst exhibited reflections of Co_3O_4 [28]. The diffractograms of the other catalysts contained the same crystallographic phases. Because the catalysts did not show any other X-ray diffraction peaks, Co_3O_4 seems to be the only crystalline cobalt species present after impregnation, drying, and calcination. No rhenium species were detected in the X-ray diffractograms, probably because of low concentration.

The only difference between the X-ray diffraction patterns of the calcined samples was the width of the Co_3O_4 peaks. Thus, the average Co_3O_4 crystallite size was dependent on the γ-Al_2O_3 support. The average spherical Co_3O_4 particle size as calculated from the (311) peak located at $2\theta = 36.9°$ are given in Table 3. Fig. 3 (filled squares) shows that the Co_3O_4 particle size clearly increased with increasing support pore size. Xiong et al. [1] also observed that the Co_3O_4 crystallite size increased with increasing γ-Al_2O_3 pore size, but that variations in the pore diameters and crystallite diameters were limited, 10.2–14.5 nm and 21.0–23.9 nm, respectively. Similar findings have been reported for silica-supported cobalt [2–8]. It also should be mentioned that no noticeable correlation was found between the BET surface areas of the supports and the Co_3O_4 particle sizes.

According to Fig. 3, the average particle size calculated from the Co_3O_4 (311) peak was larger than the average support pore diameter. Thus, most of the particles were apparently located on the exterior of the supports. However, pore diameter and Co_3O_4 particle size for location of particles should be compared with care. In fact, we believe that the particles are located inside the pore system and relate the conflicting results in Fig. 3 to the choice of pore geometry model. Because the BJH model assumes the presence of only cylindrical pores and the absence of pore networks, it oversimplifies the pore geometry. In reality, no simple pore geometry exists. Rytter et al. [41] recently used 3D-TEM and HR-TEM to visualise the pores and the cobalt–alumina interphase. A simple pore structure with the metal oxide impregnated on the walls of the pores did indeed not exist. Instead, the alumina crystals were entangled into each other in what appeared to be a chaotic fashion. Furthermore, the cobalt agglomerates stretched over a number of alumina crystals and so-called pores. Consequently, in such a case, the

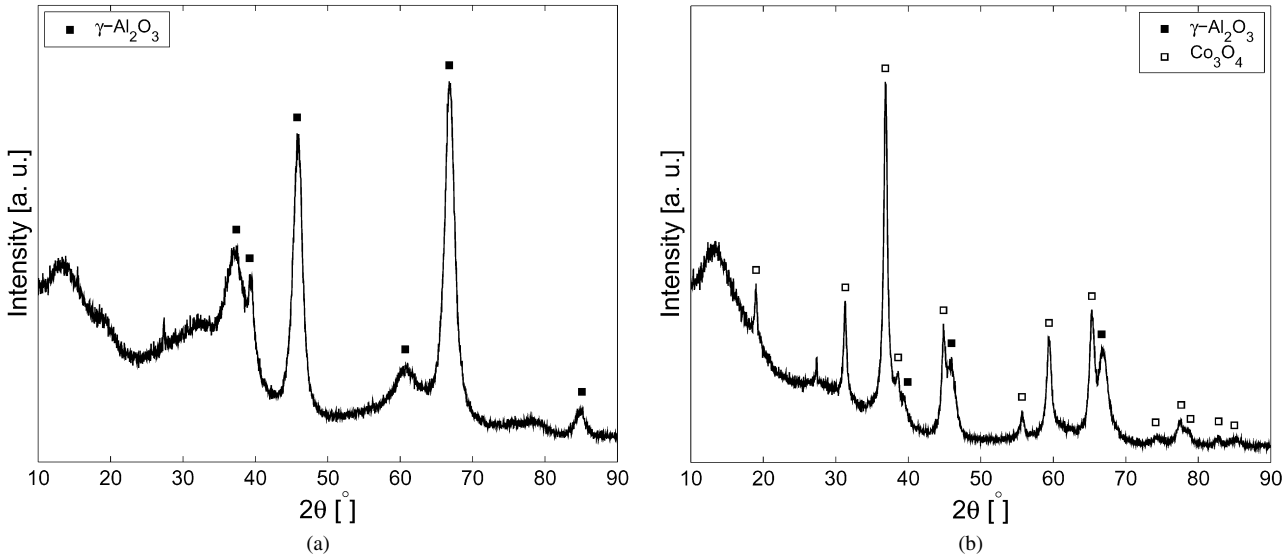

Fig. 2. X-ray diffraction patterns of support S-11 (a) and catalyst C-11 (b).

Table 3
Cobalt particle size data. The experimental error ($\pm 2\sigma$) for the Co_3O_4 particle sizes calculated from X-ray diffraction is less than ± 1 nm and is based on three independent runs for a selection of catalysts

Catalyst	X-ray diffraction		Hydrogen chemisorption	
	Co_3O_4 particle size (nm)	Co^0 particle size[a] (nm)	Cobalt dispersion (%)	Co^0 particle size[b] (nm)
C-1	16.2	12.2	8.5	11.3
C-2	15.7	11.8	9.2	10.4
C-3	16.0	12.0	8.7	11.1
C-4	18.1	13.6	8.6	11.2
C-5	21.0	15.8	7.5	12.8
C-6	18.6	14.0	8.6	11.1
C-7	20.2	15.2	7.7	12.4
C-8	19.0	14.3	8.6	11.2
C-9	19.6	14.7	8.4	11.5
C-10	22.8	17.1	7.3	13.2
C-11	19.4	14.6	7.9	12.2
C-12	25.2	18.9	7.1	13.5
C-13	28.1	21.1	6.5	14.9

The experimental error ($\pm 2\sigma$) for the cobalt metal dispersion is less than ± 0.5 nm and is based on three independent runs of all the catalysts.

[a] $d(Co^0) = 0.75 \times d(Co_3O_4)$.

[b] $d(Co^0)\ (\text{nm}) = \frac{96}{D(\%)}$.

calculated Co_3O_4 particle size can very well be larger than the calculated pore size even though the particles are located inside the pores. It also should be mentioned that particle size calculation based on the (220) Co_3O_4 reflection gave systematically slightly larger particles than the (311) reflection.

3.2. Catalyst reducibility

3.2.1. Hydrogen chemisorption

Chemisorption of hydrogen on the reduced catalysts was used to measure cobalt dispersion and calculate cobalt metal particle sizes. Uptakes of hydrogen on the supports alone were negligible. The results for the reduced catalysts, given in Table 3, show a narrow dispersion range (6.5–9.2%) and consequently a narrow particle size range (10–15 nm). However, similar to the X-ray diffraction data, Fig. 3 (open squares) indicates a positive (albeit weak) correlation between support pore diameter and cobalt particle size.

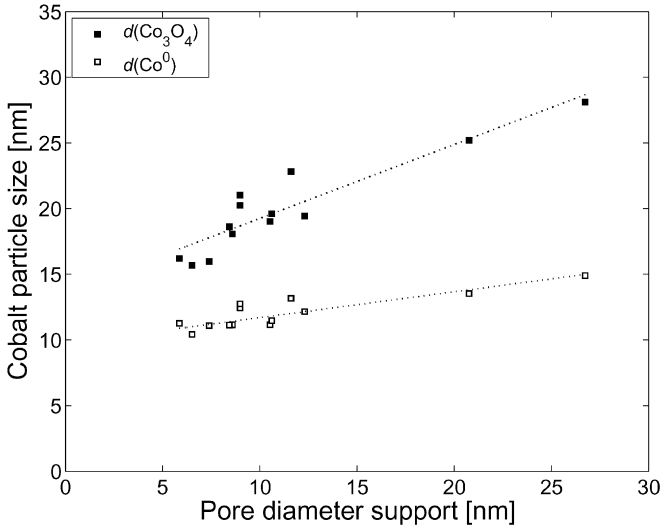

Fig. 3. Effect of the support pore diameter on the Co_3O_4 particle size calculated from X-ray diffraction data and on the metal cobalt particle size calculated from hydrogen chemisorption data.

In Fig. 3, the individual Co_3O_4 particle sizes (calculated from X-ray diffraction) almost systematically follow the individual Co^0 particle sizes (calculated from hydrogen chemisorption). However, the difference between the Co_3O_4 and Co^0 particle sizes increased with increasing support pore diameter, indicating that large cobalt oxide particles break up more easily than small particles during in situ reduction [33,34].

3.2.2. TPR

The reducibility of the oxidised samples was studied by TPR. Reduction profiles are presented in Fig. 4. The curves

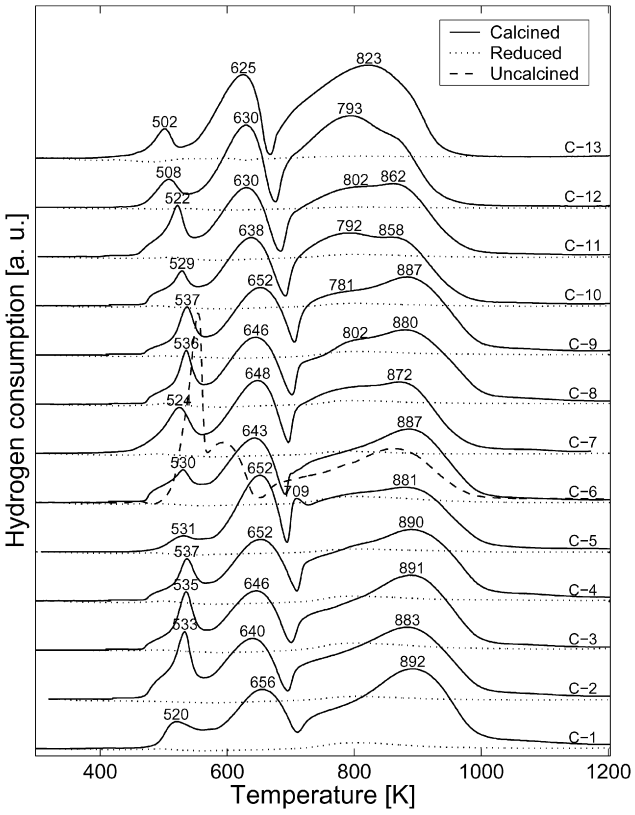

Fig. 4. Temperature-programmed reduction profiles after calcination (573 K, 16 h), after in situ reduction (623 K, 16 h), and after drying only. The uncertainty ($\pm 2\sigma$) in the location of the peak is less than ± 5 K.

recorded after calcination showed three main reduction areas, centred at approximately 530, 640, and 800 K.

The first part of the reduction process occurred between 450 and 600 K and can be attributed to the reduction of supported cobalt nitrate remaining after calcination [42]. Because calcination temperatures above 723 K are needed to completely decompose the supported cobalt nitrate [43], some nitrate will always be present in the calcined samples. To confirm the nature of the low-temperature peak, three independent sets of analyses were done. First, TPR was done both before and after calcination of one of the samples. The reduction curves of catalyst C-6 in Fig. 4 show that the area of the first peak was dramatically decreased on calcination. Second, the nitrogen contents of the uncalcined and four calcined samples were measured. Table 4 confirms that greater amounts of nitrogen were found in the uncalcined sample than in the respective calcined sample (C-6). It also indicates a correlation between the measured nitrogen amounts and the areas of the low-temperature reduction peaks for four other calcined catalysts. Third, the TPR products were analysed using a mass spectrometer. The results of catalyst C-11 are shown in Fig. 5. A clear peak of $m/e = 30$ was observed at exactly the same time that the low-temperature reduction peak appeared. This mass number corresponds to the NO^+ ion, which is the most intense fragment ion of both NO and NO_2. Based on these sets of analyses, the low-temperature peak can conclusively be ascribed to reduction of residual nitrate present after calcination.

Table 4
Area of the low-temperature TPR peak and the amount of nitrogen in the samples

Catalyst	Peak area (a.u.)	Nitrogen amount (wt%)
C-1	4.88	0.23 ± 0.05
C-2	14.71	
C-3	11.37	0.60 ± 0.08
C-4	8.31	
C-5	6.06	
C-6 uncalcined	30.40	9.5 ± 0.5
C-6	8.04	0.33 ± 0.15
C-7	12.18	
C-8	10.41	
C-9	9.19	
C-10	7.86	
C-11	10.28	0.32 ± 0.04
C-12	4.98	
C-13	4.81	

The experimental error ($\pm 2\sigma$) for the nitrogen amount is calculated from four independent runs of each sample.

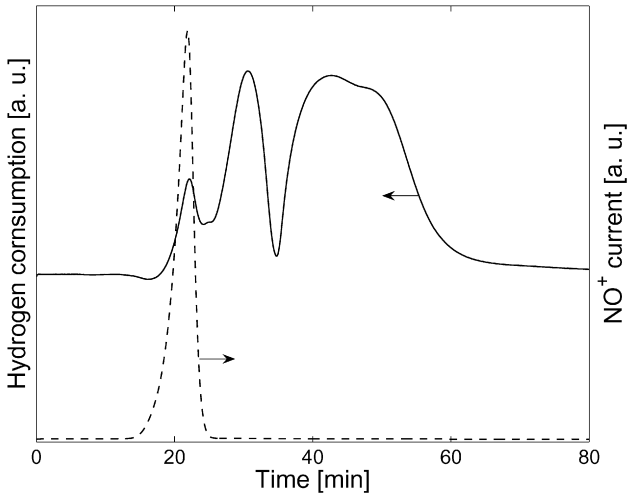

Fig. 5. Temperature-programmed reduction profile of catalyst C-11 and NO^+ ion current.

The two last peaks in Fig. 4 most likely represent a two-step reduction of Co_3O_4 to cobalt metal with CoO as an intermediate species,

$$Co_3O_4 + H_2 \rightarrow 3CoO + H_2O, \quad (3)$$

$$3CoO + 3H_2 \rightarrow 3Co^0 + 3H_2O. \quad (4)$$

Indeed, recent in situ XANES results of catalyst C-11 (labelled $20CoRe/\gamma\text{-}Al_2O_3^{\S}$ in [44]) showed that Co_3O_4 was reduced in two steps to cobalt metal with CoO as the intermediate. Co_3O_4 supported on SiO_2, TiO_2, and $\alpha\text{-}Al_2O_3$ was reduced in the same manner [44]. A two-step reduction fits well with the hydrogen consumption ratio during the two separate peaks for all of the catalysts in this study. According to the stoichiometry described by Eqs. (3) and (4), a theoretical 1:3 hydrogen consumption ratio for the two separate peaks would be expected. As shown in Table 5, all values were close, but slightly higher (0.35–0.39), probably due to poor separation of peaks or incomplete reduction of CoO. It must be mentioned that the broad

Table 5
TPR results for calcined and reduced catalyst

Catalyst	H_2 uptake during TPR of calcined catalysts (mmol/g)	H_2 uptake ratio between peak 2 and 3	H_2 uptake during TPR of reduced catalysts (mmol/g)
C-1	4.1	0.37	0.23
C-2	4.3	0.37	0.09
C-3	4.1	0.36	0.22
C-4	4.3	0.37	0.22
C-5	4.0	0.38	0.22
C-6	4.1	0.35	0.20
C-7	4.3	0.39	0.08
C-8	4.5	0.36	0.19
C-9	4.5	0.37	0.15
C-10	4.2	0.38	0.10
C-11	4.3	0.38	0.09
C-12	4.4	0.38	0.03
C-13	4.5	0.37	0.03

The experimental error ($\pm 2\sigma$) for the H_2 uptakes is approximately $\pm 4 \times 10^{-2}$ mmol/g and is based on three independent runs of catalyst C-11.

Table 6
Degree of reduction calculated from temperature-programmed reduction data and O_2 titration data

Catalyst	Degree of reduction (%)	
	TPR	O_2 titration
C-1	83	55
C-2	86	59
C-3	80	56
C-4	85	59
C-5	82	57
C-6	83	58
C-7	89	59
C-8	91	59
C-9	92	63
C-10	87	60
C-11	88	61
C-12	94	70
C-13	96	71

The experimental error ($\pm 2\sigma$) for the degree of reduction from O_2 titration is $\pm 2\%$ and is based on three independent runs of catalyst C-11.

reduction process at 700–1000 K seems to comprise more than one peak. The different shoulders appear because the catalysts consist of different-sized particles that give varying degrees of interaction with the support [45].

The reduction profiles in Fig. 4 indicate that for this catalytic system, the reduction of Co_3O_4 to CoO did not depend on the Co_3O_4 particle size, but rather occurred in the same temperature range for all of the catalysts. The same conclusion was reached by Castner et al. [46]. However, further conversion of CoO to cobalt metal appeared weakly sensitive to particle size. As shown in Fig. 4, the high-temperature reduction area shifted to slightly lower temperatures with increasing catalyst number (and pore and particle size). Lower reduction temperatures imply easier reduction and weaker metal–support interactions. The reduction spectra of catalysts C-12 and C-13 showed the strongest resemblance to the reduction profile of bulk Co_3O_4 [12].

TPR profiles were also recorded after in situ reduction in pure hydrogen (623 K, 16 h). As shown in Fig. 4, most of the cobalt oxide was transformed into metallic cobalt during reduction. For the catalysts containing many small particles, a broad but very modest reduction region centred close to 800 K was visible. Thus, after standard reduction, a small part of the cobalt phase was nonactive, giving incomplete reduction. The degrees of reduction calculated from TPR data were distributed in the interval 80–96%, as shown in Table 6.

3.2.3. Oxygen titration

The degree of reduction measured using oxygen titration at 673 K ranged from 55 to 71%, as shown in Table 6. Large particles located in wide pores were more easily reduced than small particles present in narrow pores. Weaker metal–support interactions for large particles compared with small particles is the likely reason for this [9].

The extent of reduction calculated from oxygen titration data (55–71%) was significantly lower than the degree of reduction calculated from TPR (80–96%). Moreover, X-ray absorption spectroscopy data give a higher apparent degree of reduction than oxygen titration data [44]. We have previously suggested that incomplete oxidation of the reduced catalysts with oxygen pulses is the cause of this [44]. Khodakov et al. [6] also indicated that oxygen titration may underestimate the extent of reduction. They showed that in an inert atmosphere at temperatures above 623 K, the supported CoO phase could be more stable than Co_3O_4 [9]. Thus, oxygen titration conducted in helium at 673 K could result in oxidation of cobalt metal phases to CoO instead of Co_3O_4 or to a mixture of CoO and Co_3O_4 [6].

3.3. Fischer–Tropsch synthesis

The Fischer–Tropsch synthesis produces a wide range of hydrocarbons, consisting of linear and branched paraffins and olefins, and oxygenates. However, the distribution of these hydrocarbons is highly dependent on the reaction conditions and catalyst. The compounds are produced in a polymerisation mechanism in which a one-carbon unit is added to the growing chain. A growing chain can terminate either by H-abstraction to give α-olefins or by hydrogenation to give n-paraffins. Secondary reactions add further complexity to the Fischer–Tropsch synthesis. Hydrogenation and readsorption of primary olefins represent the main secondary reactions. In addition, the pores are filled with wax and water, which slows pore diffusivity significantly. Diffusion limitations may results from limitation of the arrival of CO to the active points or through the limited removal of reactive products [15].

To conclude, it is reasonable to say that because of the complex nature of the Fischer–Tropsch synthesis, any study of the catalytic performance of similar catalysts requires strict control of reaction conditions. For this reason, all catalysts were subjected to the same reactor setup and gaseous environment during synthesis. The Fischer–Tropsch synthesis measurements were done at $T = 483$ K, $P = 20$ bar, and $H_2/CO = 2.1$. Fischer–Tropsch synthesis inactivity of the reactor system, silicon carbide, and γ-Al_2O_3 was confirmed in three separate runs. To find an appropriate catalyst particle size, in one of the catalysts Fischer–Tropsch synthesis was run with different catalyst

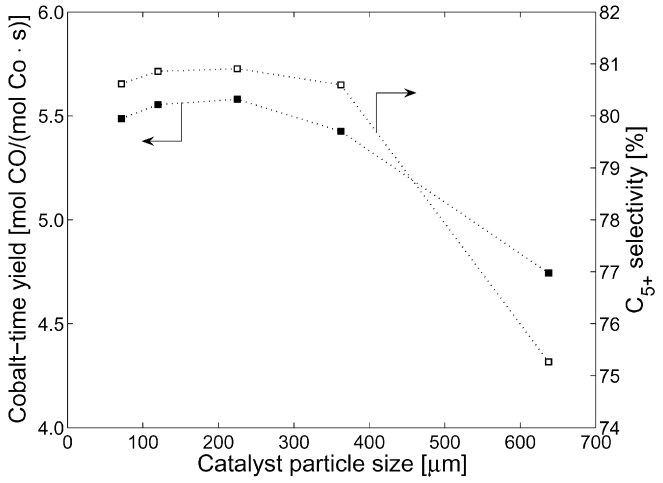

Fig. 6. Effect of the catalyst particle size on the hydrocarbon production and C_{5+} selectivity of catalyst C-3 at 483 K, 20 bar, $H_2/CO = 2.1$. The C_{5+} selectivity was recorded at 50% CO conversion.

Table 7
Cobalt-time yields and site-time yields calculated after 8 h on stream (T = 483 K, P = 20 bar, $H_2/CO = 2.1$, and GHSV = 15 Nl/(g_{cat} × h))

Catalyst	Cobalt-time yield ×10^3 (mol CO/(mol Co × s))	Site-time yield ×10^3 (s^{-1})
C-1	5.3	62
C-2	4.6	50
C-3	5.9	68
C-4	4.4	51
C-5	3.4	45
C-6	5.4	62
C-7	5.6	73
C-8	4.6	53
C-9	5.1	61
C-10	4.7	65
C-11	5.3	67
C-12	4.6	65
C-13	4.1	63

The experimental error ($\pm 2\sigma$) for the site-time yield is $\pm 5 \times 10^{-3}$ s^{-1} based on three independent runs of catalyst C-11.

particle sizes, as shown in Fig. 6. For catalyst C-3, both the activity and the selectivity were (within experimental error) unaffected by the catalyst particle size in the range of 53–225 µm. But catalytic performance was poorer for larger catalyst particles, most likely due to mass transfer limitations. Fig. 6 also shows that the effect of increasing particle size is more pronounced on the C_{5+} selectivity than on the rate. The results are in qualitative agreement with findings of Hilmen et al. [47]. In summary, because the results in this work were obtained on 53–90 µm catalyst particles, we can reasonably conclude that no diffusion limitations existed.

3.3.1. Fischer–Tropsch synthesis activity

Cobalt-time yields and site-time yields calculated after 8 h on stream are given in Table 7. The small variations in site-time yield (45–73 × 10^{-3} s^{-1}) could be related to the chemical purity of the catalyst samples. As shown in Fig. 7, the site-time yield is correlated with the sodium content, and it is reasonable to assume that the presence of sodium has a negative impact on site-time yield. For catalysts containing approximately the same amount of sodium, the site-time yield was constant at 62–73 × 10^{-3} s^{-1} (within the combined experimental error of the chemisorption and activity measurements). Furthermore, there was no correlation between the cobalt-time yield or site-time yield and the physical parameters of the catalysts (e.g., surface area, pore diameter, and pore volume). Finally, it should be mentioned that the site-time yields obtained for promoted and unpromoted cobalt catalysts deposited on γ-Al_2O_3, SiO_2, and TiO_2 at 483 K and 20 bar by Storsæter et al. [14] are in the same range as the site-time yields presented in this paper.

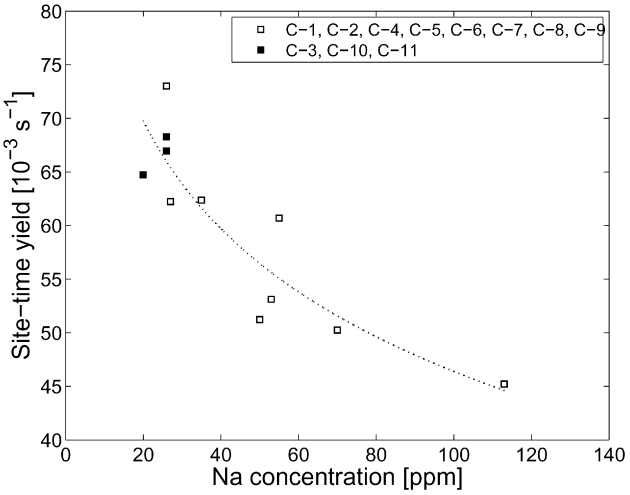

Fig. 7. Effect of the catalyst concentration of Na on the site-time yield measured after 8 h on stream at 483 K, 20 bar, and $H_2/CO = 2.1$.

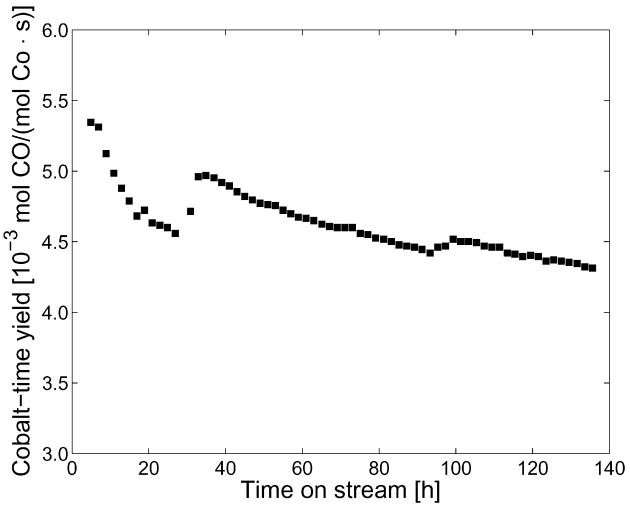

Fig. 8. Hydrocarbon production rate of catalyst C-11 at 483 K, 20 bar, and $H_2/CO = 2.1$.

Fig. 8 presents cobalt-time yields for catalyst C-11. The space velocity was decreased after 26 h on stream to reach a target value of 50% CO conversion. A small positive change in the catalytic productivity was observed for all of the catalysts when the conversion and, accordingly, the water concentration increased. Small amounts of water are probably helpful to CO conversion. The catalysts were kept on stream for 130 h. As

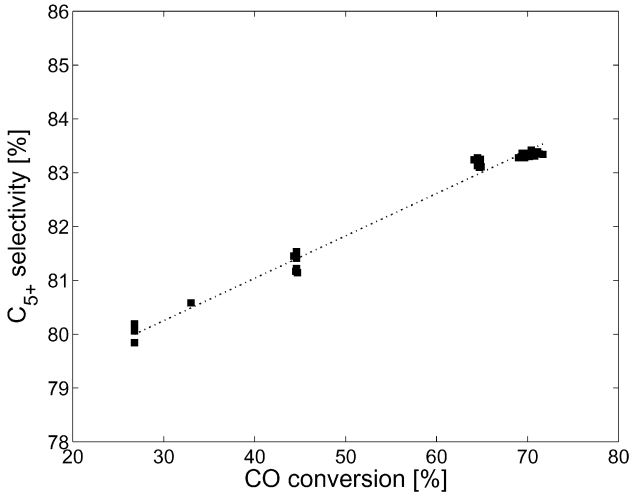

Fig. 9. Effect of the CO conversion on the C_{5+} selectivity for catalyst C-11 at 483 K, 20 bar, and $H_2/CO = 2.1$. The CO conversion was adjusted varying the space velocity (GHSV = 15.0, 12.0, 9.0, 6.0, 4.9 Nl/(g_{cat} × h)).

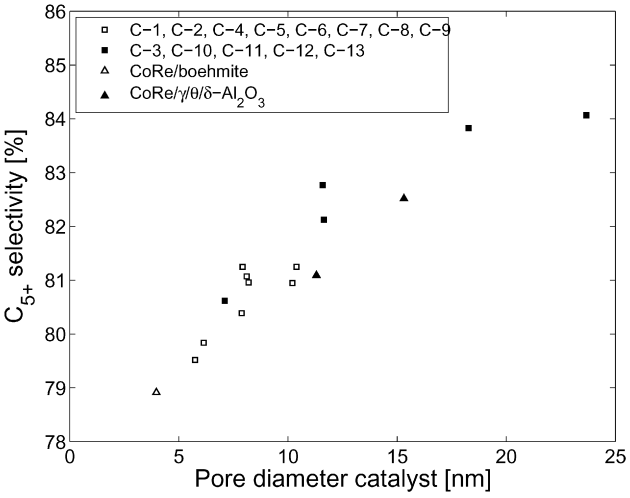

Fig. 10. Effect of the catalyst pore diameter on the C_{5+} selectivity at 483 K, 20 bar, $H_2/CO = 2.1$, and 50% CO conversion.

shown in Fig. 8, the catalyst deactivated with time on stream due to sintering, surface cobalt oxidation, or solid-state reactions rendering inactive cobalt. Whereas oxidation of cobalt has long been postulated as a deactivation mechanism [48], Saib et al. [49] recently ruled out oxidation for cobalt particles ⩾6 nm in diameter.

3.3.2. Fischer–Tropsch synthesis selectivity

As shown in Fig. 9, it is important to compare the product selectivity of different catalysts at the same conversion level. The relationship was obtained for catalyst C-11 by changing the space velocity of synthesis gas to reach different conversion levels. We believe that the increase in C_{5+} selectivity with increasing CO conversion can be related to the increased amount of water with increasing conversion. Separate experiments on catalysts C-1 to C-13 have in fact shown that the external addition of water increases C_{5+} selectivity [50]. To the best of our knowledge, the first investigation dealing with the effect of water on the catalytic performance was reported in 1985 by Minderhoud et al. [51]. These authors observed that the addition of steam increased the C_{9+} selectivity of cobalt supported on Al_2O_3 and TiO_2. Consequently, the hydrocarbon selectivities presented in Table 7 were recorded at the same conversion level. The experimental conversion was always between 48 and 52%, but to further increase the precision of the comparisons, the selectivities were extrapolated or interpolated to exactly 50% conversion. The response of C_{5+} selectivity to variations in the CO conversion level was similar for all the samples. Thus, we believe that the C_{5+} selectivity at 50% conversion is representative for the ability of the different catalysts to produce long-chain hydrocarbons also at higher conversions.

Interestingly, Fig. 10 shows that C_{5+} selectivity can be increased by choosing a starting support that contains wide pores. The increased C_{5+} selectivity is a result of both decreased methane and C_2–C_4 selectivity (Table 8). Thus, wide-pore catalysts have a higher chain-growth probability (α) than narrow-pore catalysts. We believe that this conclusion is valid and not

Table 8
Selectivity data at $T = 483$ K, $P = 20$ bar, $H_2/CO = 2.1$, and 50% CO conversion. The experimental error ($\pm 2\sigma$) for the C_{5+} selectivity is ±0.5%

Catalyst	GHSV Nl/(g_{cat} × h))	Hydrocarbon selectivity (%)							
		C_1	$C_2=$	C_2-	$C_3=$	C_3-	$C_4=$	C_4-	C_{5+}
C-1	8.4	9.8	0.10	0.92	2.81	1.60	2.49	2.14	79.5
C-2	7.6	9.5	0.11	0.97	2.86	1.56	2.66	2.08	79.8
C-3	9.5	9.3	0.09	0.81	2.66	1.39	2.59	1.99	80.6
C-4	7.3	9.8	0.09	0.92	2.59	1.46	2.17	1.92	80.4
C-5	6.1	10.1	0.06	0.82	2.05	1.39	1.87	1.90	81.3
C-6	9.3	9.1	0.09	0.79	2.70	1.30	2.50	1.85	81.1
C-7	9.1	10.0	0.07	0.86	2.27	1.39	2.06	1.84	81.0
C-8	7.4	9.6	0.08	0.92	2.37	1.42	2.19	1.87	80.9
C-9	7.7	9.3	0.08	0.80	2.47	1.27	2.32	1.74	81.2
C-10	7.5	8.8	0.07	0.84	2.12	1.30	1.88	1.72	82.8
C-11	8.9	9.0	0.08	0.80	2.37	1.26	2.18	1.72	82.1
C-12	7.9	8.4	0.07	0.80	1.98	1.15	1.81	1.46	83.8
C-13	6.5	8.5	0.06	0.98	1.79	1.10	1.65	1.26	84.1

The uncertainty is based on three independent runs of catalyst C-10.

a result of the variations in sodium content. In fact, five catalysts (C-1, C-3, C-7, C-10, and C-11) that contained practically the same amount of sodium showed significant variations in C_{5+} selectivity. Storsæter et al. [14] also obtained a positive (albeit weak) positive correlation between pore diameter and C_{5+} selectivity; however, that work was done on different supports (i.e., γ-Al_2O_3, SiO_2, and TiO_2) and may be a result of different chemical identity. Saib et al. [3] and Song and Li [8] reported that the selectivity passed through a maximum located at 10 and 6.6 nm, respectively. Saib et al. [3] explained the maximum quantitatively using the transport model of Iglesia et al. [15,22,23]. As shown in Fig. 10, no such maximum was observed in the present work. This is not surprising, because the intraparticle diffusion limitations were very similar for all of the samples studied in this work. Indeed, the structural parameter, χ, for these catalysts introduced by Iglesia et al. [15,22,23] was calculated to be in the narrow range of 10–23 × 10^{-16} m. The relationship between pore diameter and selectivity may be related to the extent of α-olefin readsorption; however, because no relationship between olefin/paraffin ratios and prod-

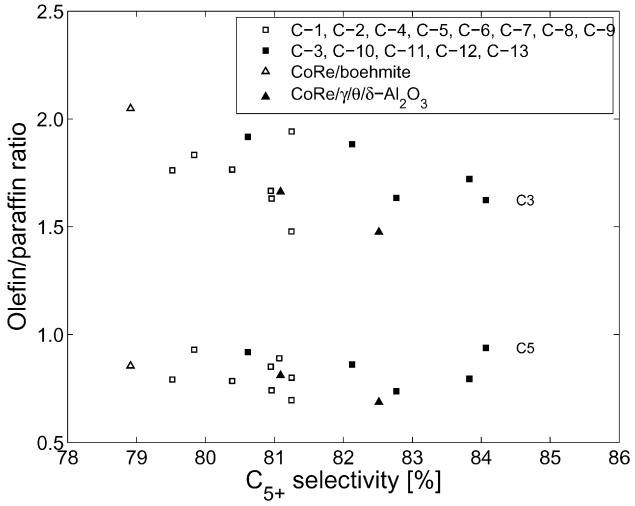

Fig. 11. Olefin/paraffin ratios for C_3 and C_5 hydrocarbons at 483 K, 20 bar, $H_2/CO = 2.1$, and 50% CO conversion.

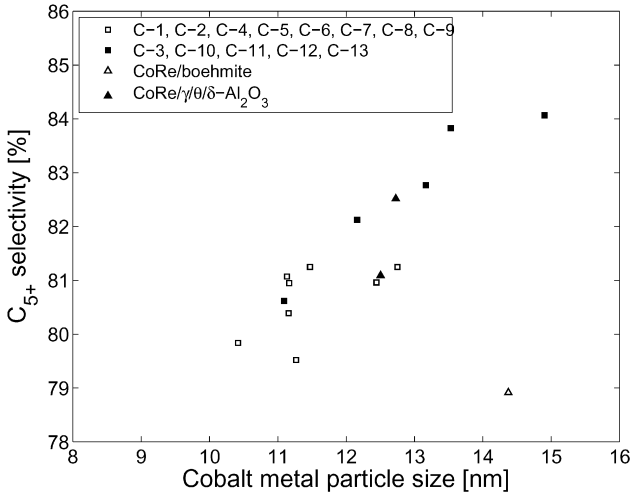

Fig. 12. Effect of the cobalt particle size on the C_{5+} selectivity at 483 K, 20 bar, $H_2/CO = 2.1$, and 50% CO conversion.

uct selectivity was found (Fig. 11), limited removal of active α-olefin products probably cannot explain the relatively large variations in C_{5+} selectivity obtained for the different catalysts. Furthermore, Fig. 10 shows the highest C_{5+} selectivity for the wide-pore based catalysts in which the product transport actually should be the least restricted and, accordingly, in which the residence time available for olefin readsorption should be the shortest. Shi and Davis [24] also demonstrated that diffusional limitations for the olefin products and their subsequent reincorporation as chain initiators do not have a major impact on the product distribution. Based on these results, we believe that the pore diameter cannot alone explain the variations in C_{5+} selectivity.

Because the cobalt particle size increases with increasing pore diameter, the C_{5+} selectivity also increases with increasing cobalt particle size, as illustrated in Fig. 12. The cobalt particle sizes in Fig. 12 were not corrected for degree of reduction; however, the same trend is obtained if the degrees of reduction listed in Table 6 are taken into account. Bezemer et al. [21] also recently found that cobalt particle size affected C_{5+} selectivity, most strongly for particles <8 nm in diameter. In contrast, however, we find a relationship between the cobalt particle size and the C_{5+} selectivity even for particles >8 nm. Moreover, Storsæter et al. [14] observed very high selectivity for cobalt supported on TiO_2, with an average cobalt particle size of 40 nm.

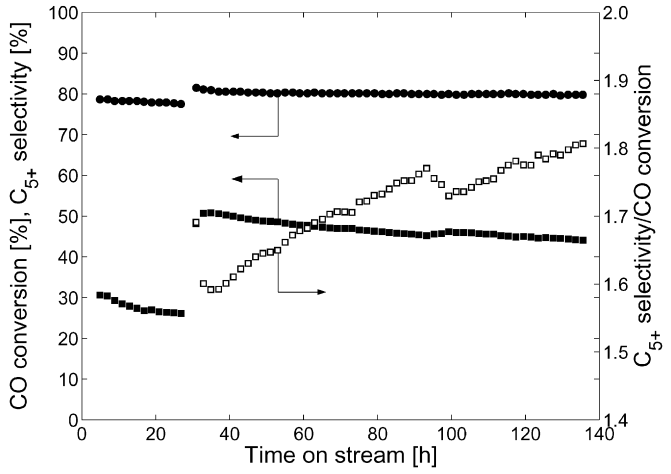

Fig. 13. CO conversion and C_{5+} selectivity of catalyst C-11 at 483 K, 20 bar, and $H_2/CO = 2.1$.

Fig. 13 further illustrates that particle size is an important factor in product selectivity. Even though CO conversion decreased with time on stream, the catalyst gave similar C_{5+} selectivity, which is surprising based on the results shown in Fig. 9. Indeed, Fig. 13 shows that the ratio between the selectivity and conversion increased with time on stream for catalyst C-11. We believe that this phenomenon can be explained by an increase in the average cobalt particle size because of deactivation. Both sintering and oxidation of small cobalt particles increase the average cobalt particle size. It is likely that the increased average cobalt particle size of catalyst C-11 gave higher C_{5+} selectivity, which counteracted the decrease in selectivity due to lower CO conversion. Accordingly, the ratio between the selectivity and conversion increased.

We also speculate that the particle size evolution during in situ reduction may be important for the product distribution. According to Rytter et al. [33,34], the Co_3O_4 particles break up during in situ reduction. Fig. 14 shows the ratio between the diameter of the Co_3O_4 particle (X-ray diffraction) and the diameter of the corresponding Co^0 metal particle size (H_2 chemisorption). We speculate that this ratio is related to the number of crystal boundaries in the catalyst after in situ reduction and that a high number is favourable for C_{5+} selectivity. It is striking that the Puralox-based catalysts all lay along one line.

Summarising, explaining the variations in C_{5+} selectivity with diffusion effects is difficult, and we are left with the possibility that the cobalt particle size and possibly shape control the product distribution. A particle size-dependent C_{5+} selectivity is in agreement with the recent findings of Bezemer et al. [21]; however, we have been able to extend their results to larger cobalt particles.

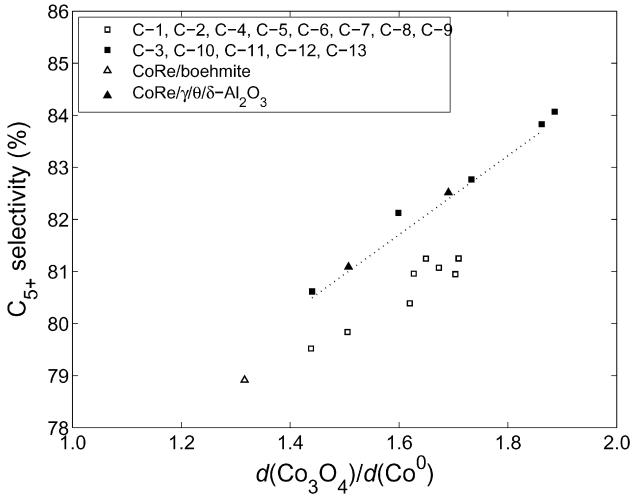

Fig. 14. Effect of cobalt particle break-up on the C_{5+} selectivity at 483 K, 20 bar, $H_2/CO = 2.1$, and 50% CO conversion.

4. Conclusion

Numerous γ-Al_2O_3-supported catalysts containing 20 wt% Co and 0.5 wt% Re were prepared and characterised by different techniques. Incipient wetness impregnation gave a clear positive relationship between support pore size and cobalt particle size. The effect of support variables on the Fischer–Tropsch synthesis activity and selectivity was investigated in a fixed-bed reactor. Interestingly, the Fischer–Tropsch data demonstrate a strong relationship between the starting support and the final activity and selectivity. The data also show that the cobalt particle size is of primary importance for the product selectivity.

Acknowledgments

Financial support was provided by the Norwegian Research Council through the KOSK programme. The authors thank Statoil ASA for providing financial support and supplying the alumina samples. They also thank Bjørn Christian Enger for helpful comments on the manuscript and Ether Ochoa Fernández for assistance with the experiments.

References

[1] H. Xiong, Y. Zhang, S. Wang, J. Li, Catal. Commun. 6 (2005) 512.
[2] D.G. Castner, P.R. Watson, I.Y. Chan, J. Phys. Chem. 93 (1989) 3188.
[3] A.M. Saib, M. Claeys, E. van Steen, Catal. Today 71 (2002) 395.
[4] A.Y. Khodakov, A. Griboval-Constant, R. Bechara, F. Villain, J. Phys. Chem. B 105 (2001) 9805.
[5] A.Y. Khodakov, R. Bechara, A. Griboval-Constant, Stud. Surf. Sci. Catal. 142 (2002) 1133.
[6] A.Y. Khodakov, A. Griboval-Constant, R. Bechara, V.L. Zholobenko, J. Catal. 206 (2002) 230.
[7] A.Y. Khodakov, R. Bechara, A. Griboval-Constant, Appl. Catal. A 254 (2003) 273.
[8] D. Song, J. Li, J. Mol. Catal. A 247 (2006) 206.
[9] A.Y. Khodakov, J. Lynch, D. Bazin, B. Rebours, N. Zanier, B. Moisson, P. Chaumette, J. Catal. 168 (1997) 16.
[10] S.L. Soled, E. Iglesia, R.A. Fiato, J.E. Baumgartner, H. Vroman, S. Miseo, Top. Catal. 26 (2003) 101.
[11] C.H. Mauldin, United States Patent 4,568,663 (1986), to Exxon Research and Engineering Co.
[12] A.M. Hilmen, D. Schanke, A. Holmen, Catal. Lett. 38 (1996) 143.
[13] D. Schanke, S. Eri, E. Rytter, C. Aaserud, A.-M. Hilmen, O.A. Lindvåg, E. Bergene, A. Holmen, Stud. Surf. Sci. Catal. 147 (2004) 301.
[14] S. Storsæter, Ø. Borg, E.A. Blekkan, A. Holmen, J. Catal. 231 (2005) 405.
[15] E. Iglesia, S.L. Soled, R.A. Fiato, J. Catal. 137 (1992) 212.
[16] E. Iglesia, Stud. Surf. Sci. Catal. 107 (1997) 153.
[17] E. Iglesia, Appl. Catal. A 161 (1997) 59.
[18] R. Oukaci, A.H. Singleton, J.G. Goodwin Jr., Appl. Catal. A 186 (1999) 129.
[19] C.J. Bertole, C.A. Mims, G. Kiss, P. Joshi, Stud. Surf. Sci. Catal. 136 (2001) 369.
[20] C.J. Bertole, C.A. Mims, G. Kiss, J. Catal. 221 (2004) 191.
[21] G.L. Bezemer, J.H. Bitter, H.P.C.E. Kuipers, H. Oosterbeek, J.E. Holewijn, X. Xu, F. Kapteijn, A.J. van Dillen, K.P. de Jong, J. Am. Chem. Soc. 128 (2006) 3956.
[22] E. Iglesia, S.C. Reyes, R.J. Madon, S.L. Soled, Adv. Catal. 39 (1993) 221.
[23] E. Iglesia, S.L. Soled, R.A. Fiato, G.H. Via, Stud. Surf. Sci. Catal. 81 (1994) 433.
[24] B. Shi, B.H. Davis, Catal. Today 106 (2005) 129.
[25] S. Brunauer, P.H. Emmett, E. Teller, J. Am. Chem. Soc. 60 (1938) 309.
[26] E.P. Barrett, L.G. Joyner, P.P. Halenda, J. Am. Chem. Soc. 73 (1951) 373.
[27] Lowell, Shields, Thomas, Thommes, Characterisation of Porous Solids and Powders: Surface Area, Pore Size and Density, Kluwer Academic, Dordrecht, 2004, p. 117.
[28] DIFFRACplus EVA Release 2001 Version 7.0 rev.0, Bruker AXS (2001).
[29] P. Scherrer, Göttingen Nachrichten 2 (1918) 98.
[30] W.L. Bragg, The Crystalline State: A General Survey, vol. 1, Bell & Sons, London, 1949, p. 189.
[31] J.L. Lemaitre, P. Govind Menon, F. Delannay, in: F. Delannay (Ed.), Characterisation of Heterogeneous Catalysts, Dekker, New York, 1984, pp. 299–365.
[32] D. Schanke, S. Vada, E.A. Blekkan, A.M. Hilmen, A. Hoff, A. Holmen, J. Catal. 156 (1995) 85.
[33] E. Rytter, D. Schanke, S. Eri, H. Wigum, T.H. Skagseth, N. Sincadu, Proc. Am. Chem. Soc. Div. Pet. Chem. 49 (2004) 182.
[34] E. Rytter, D. Schanke, S. Eri, H. Wigum, T.H. Skagseth, E. Bergene, in: Proc. CatCon2005, 2005.
[35] R.C. Reuel, C.H. Bartholomew, J. Catal. 85 (1984) 63.
[36] R.D. Jones, C.H. Bartholomew, Appl. Catal. 39 (1988) 77.
[37] E.A. Blekkan, A. Holmen, S. Vada, Acta Chem. Scand. 47 (1993) 275.
[38] C.H. Bartholomew, R.J. Farrauto, J. Catal. 45 (1976) 41.
[39] A.-M. Hilmen, E. Bergene, O.A. Lindvåg, D. Schanke, S. Eri, A. Holmen, Catal. Today 105 (2005) 357.
[40] E. Rytter, S. Eri, International Publication Number WO 2006/010936 A1 (2006), to Statoil ASA and PetroSA.
[41] E. Rytter, D. Schanke, S. Eri, H. Wigum, T.H. Skagseth, E. Bergene, In: Abstracts of Papers of 229th ACS National Meeting, 2005.
[42] A. Lapidus, A. Krylova, V. Kazanskii, V. Borovkov, A. Zaitsev, J. Rathousky, A. Zukal, M. Jančálková, Appl. Catal. 73 (1991) 65.
[43] Ø. Borg, E.A. Blekkan, S. Eri, D. Akporiaye, B. Vigerust, E. Rytter, A. Holmen, Top. Catal. (2007), doi:10.1007/s11244-002007-0237-1.
[44] Ø. Borg, M. Rønning, S. Storsæter, W. van Beek, A. Holmen, Stud. Surf. Sci. Catal. 163 (2007) 255.
[45] G. Jacobs, T.K. Das, Y. Zhang, J. Li, G. Racoillet, B.H. Davis, Appl. Catal. A 233 (2002) 263.
[46] D.G. Castner, P.R. Watson, I.Y. Chan, J. Phys. Chem. 94 (1990) 819.
[47] A.-M. Hilmen, E. Bergene, O.A. Lindvåg, D. Schanke, S. Eri, A. Holmen, Stud. Surf. Sci. Catal. 130 (2000) 1163.
[48] A.M. Hilmen, D. Schanke, K.F. Hanssen, A. Holmen, Appl. Catal. A 186 (1999) 169.
[49] A.M. Saib, A. Borgna, J. van de Loosdrecht, P.J. van Berge, J.W. Niemantsverdriet, Appl. Catal. A 312 (2006) 12.
[50] Ø. Borg, S. Storsæter, S. Eri, H. Wigum, E. Rytter, A. Holmen, Catal. Lett. 107 (2006) 95.
[51] J.K. Minderhoud, M.F.M. Post, S.T. Sie, E.J.R. Sudhoelter, United States Patent 4,628,133 (1986), to Shell Internationale Research.